Journal of Solid Mechanics Vol. 10, No. 2 (2018) pp. 435-449

Thermoelastic Fracture Parameters for Anisotropic Plates

S. Kebdani [1,*], A. Sahli [1,2] , S. Sahli [2]

[1]*Laboratoire de Mécanique Appliquée , Université des Sciences et de la Technologie d'Oran , Alegria*
[2]*Laboratoire de Recherche des Technologies Industrielles , Université Ibn Khaldoun de Tiaret , Alegria*

Received 24 March 2018; accepted 20 May 2018

ABSTRACT

This paper deals with the determination of the effect of varying material properties on the value of the stress intensity factors, K_I and K_{II}, for anisotropic plates containing cracks and subjected to a temperature change. Problems involving cracks and body forces, as well as thermal loads are analysed. The quadratic isoperimetric element formulation is utilized, and SIFs may be directly obtained using the 'traction formula' and the 'displacement formula'. Three cracked plate geometries are considered in this study, namely: (1) a plate with an edge-crack; (2) a plate with a double edge-crack; (3) a plate with symmetric cracks emanating from a central hole. Where appropriate, finite element method (FEM) analyses are also performed in order to validate the results of the BEM analysis. The results of this study show that, for all crack geometries, the mode-I stress intensity factor, $K*I$ decreases as the anisotropy of the material properties is increased. Additionally, for all these cases, $K*I$ decreases as the angle of orientation of the material properties, θ , increases with respect to the horizontal axis. The results also show that BEM is an accurate and efficient method for two-dimensional thermoelastic fracture mechanics analysis of cracked anisotropic bodies.

Keywords : Boundary element method; Stress intensity factors; Anisotropy.

1 INTRODUCTION

OVER the past couple of decades, anisotropic materials have become more commonly used in the aerospace industry as a primary structural material in applications such as satellites and aircraft. In the aerospace industry, a major design consideration is the presence and behavior of cracks. As a result, much research has been conducted in the past two decades to study cracked anisotropic structures subjected to various types of mechanical loads, and much is now known about their behavior. However, in many cases, these structures are also subjected to thermal loads. There has, however, been very little research done to determine the effects anisotropic material properties have on the fracture behavior of a cracked body subjected to a temperature change. The goal of the present study is to examine some of these effects.

The early groundwork for linear elastic fracture mechanics (LEFM) analysis in plane anisotropy was performed by [1] used the modified mapping collocation (MMC) method to express the stresses and displacements in the crack-tip vicinity in terms of the mode-I stress intensity factor (SIF) for a two-dimensional anisotropic body [2] used the

*Corresponding author. Tel.: +213 557477900.
E-mail address: mechanics184@yahoo.com (S.Kebdani).

MMC method to determine the mode-I stress intensity factor, K_I, for a plane orthotropic body with a central-crack, while [3] also used the same technique to analyze a plane orthotropic body with a slant-crack. Although [4] had presented, for the first time, a BEM formulation for plane anisotropy, no fracture mechanics analysis was carried out at this time[5] followed this groundwork with an alternative formulation for two-dimensional anisotropic fracture mechanics based on modified Green's functions. This new formulation had the distinct advantage that the crack itself did not need to be modeled. However, it was only applicable to straight cracks and relatively simple geometric configurations.

Most major work in the area of two-dimensional LEFM analysis of anisotropic bodies in more recent years has been split between two main groups, the dual boundary element method (DBEM) along with its various forms, and the sub-regioning approach. DBEM [6]; [7] is a single domain approach, which instead of sub-regioning the solution domain, models the tractions on one crack face, and displacements on the other, to avoiding discontinuities which arise here. [8] Propose two quantitative thermoelastic strain analysis (TSA) experimental methods to determine the surface strain fields in mechanically loaded orthotropic materials using the spatial distribution of temperature gradient measured from the surface. The general applicability of the BEM algorithm for fracture mechanics applications is demonstrated by three crack problems with slanted cracks in [9]. [10] Develops the Somigliana type boundary integral equations for fracture of anisotropic thermoelastic solids using the Stroh formalism and the theory of analytic functions. Stress intensity factors, K_I and K_{II}, for inclined cracks are determined in a uniaxially-loaded orthotropic graphite–epoxy composite using measured temperatures and least-squares by [11]. [12] Develop a new computational method based on the equivalent domain integral (EDI) for mode-I fracture analysis of orthotropic functionally graded materials (FGMs) subjected to thermal stresses. The formulation for DBEM is complicated, but the ability to model cracks without subregioning makes this method very well suited to the study of crack propagation. For the straightforward determination of SIFs only, the sub-regioning, or multiple domain, approach is still the simplest. With this method the sub-regioned body is analyzed, and the stresses and displacements near the crack-tip can be used to determine the SIFs with the now well established 'traction formula' and/or 'displacement formula' [13]. It should be noted that other methods have been proposed for calculating SIFs which may also be applicable to two-dimensional anisotropic LEFM, such as the J_k integral [14,15], weight functions [16], and a singularity subtraction technique [17]. They are mathematically more involved and require significant modifications and implementation into a BEM computer code.

There has been relatively little amount of work done in the area of two dimensional thermoelastic fracture mechanics analysis for anisotropic bodies using BEM. This is due to the presence of extra volume integrals in the integral equations which arise when thermal effects are present, and the subsequent difficulty in transforming these volume integrals into surface integrals. In elasticity analysis, thermal loads are often treated as 'pseudo-body forces' because their terms appear together with those for body forces in the governing differential equation [18]. The presence of volume integrals, however, destroys the main feature of the boundary element method as a boundary solution method, and therefore, transformation of these domain integrals is necessary to restore the method to a truly 'boundary-only' technique. This transformation was first achieved for body force loading by [19, 20] when they developed the exact transformation method (ETM) for body forces in two-dimensional anisotropy in BEM, and applied the formulation to analyze crack problems. Note that body forces have also been treated earlier using the particular integral method (PIM) [21], but for anisotropy, the approach is an approximate one. [22] Subsequently developed a direct domain mapping technique to solve two-dimensional anisotropic field problems in BEM.

This work facilitated the transformation of the thermoelastic domain integral into surface integrals by [23] when they developed the ETM for two-dimensional thermoelastic anisotropy in BEM. This formulation was extended to allow for determination of interior point stresses [24], and employed for fracture mechanics analysis [25]. Other attempts using BEM to deal with anisotropic thermoelasticity have been made by [26]; and [27] using PIM, but this method is not general and has not been applied to crack problems.

This paper presents results of two dimensional thermoelastic fracture mechanics analysis of cracked anisotropic bodies using the BEM based on the exact transformation method (ETM). Problems involving cracks, body forces, as well as thermal loads are analyzed. The quadratic Isoperimetric element formulation is utilized, and stress intensity factors (SIFs) may be directly obtained using the 'traction formula' and the 'displacement formula'. Only the case of uniform temperature distribution was considered in this study. The effect of varying material properties and varying material orientation of these material properties on the value of the SIFs for cracked rectangular plates under mode-I conditions is investigate.

2 ANISOTROPIC STRESS AND DISPLACEMENT FIELD NEAR A CRACK TIP

The stress and displacement expressions in the neighborhood of the crack tip in homogeneous anisotropic media under a plane stress condition with zero body forces are given by [28] as:

$$\sigma_x = \frac{K_I}{\sqrt{r}}\mathrm{Re}\left[\frac{s_1 s_2}{s_1 - s_2}\left(\frac{s_2}{z_2} - \frac{s_1}{z_1}\right)\right] + \frac{K_{II}}{\sqrt{r}}\mathrm{Re}\left[\frac{1}{s_1 - s_2}\left(\frac{s_2^2}{z_2} - \frac{s_1^2}{z_1}\right)\right] \tag{1}$$

$$\sigma_y = \frac{K_I}{\sqrt{r}}\mathrm{Re}\left[\frac{1}{s_1 - s_2}\left(\frac{s_2}{z_2} - \frac{s_1}{z_1}\right)\right] + \frac{K_{II}}{\sqrt{r}}\mathrm{Re}\left[\frac{1}{s_1 - s_2}\left(\frac{1}{z_2} - \frac{1}{z_1}\right)\right] \tag{2}$$

$$\tau_{xy} = \frac{K_I}{\sqrt{r}}\mathrm{Re}\left[\frac{s_1 s_2}{s_1 - s_2}\left(\frac{1}{z_2} - \frac{1}{z_1}\right)\right] + \frac{K_{II}}{\sqrt{r}}\mathrm{Re}\left[\frac{1}{s_1 - s_2}\left(\frac{s_2}{z_2} - \frac{s_1}{z_1}\right)\right] \tag{3}$$

and

$$u = K_I\sqrt{r}\,\mathrm{Re}\left[\frac{1}{s_1 - s_2}\left(s_1 p_2 z_2 - s_2 p_1 z_1\right)\right] + K_{II}\sqrt{r}\,\mathrm{Re}\left[\frac{1}{s_1 - s_2}\left(p_2 z_2 - p_1 z_1\right)\right] \tag{4}$$

$$v = K_I\sqrt{r}\,\mathrm{Re}\left[\frac{1}{s_1 - s_2}\left(s_1 q_2 z_2 - s_2 q_1 z_1\right)\right] + K_{II}\sqrt{r}\,\mathrm{Re}\left[\frac{1}{s_1 - s_2}\left(q_2 z_2 - q_1 z_1\right)\right] \tag{5}$$

with

$$z_1 = \sqrt{\cos\theta + s_1 \sin\theta} \qquad z_2 = \sqrt{\cos\theta + s_2 \sin\theta}$$
$$p_1 = a_{11}s_1^2 + a_{12} - a_{16}s_1 \qquad p_2 = a_{11}s_2^2 + a_{12} - a_{16}s_2$$
$$q_1 = a_{11}s_1 + \frac{a_{22}}{s_1} - a_{26} \qquad q_2 = a_{11}s_2 + \frac{a_{22}}{s_2} - a_{26}$$

where Re denotes the real part of the complex function between brackets. s_1, s_2 and their conjugates are roots of the fourth order characteristic equation

$$a_{11}s^4 + 2a_{16}s^2 + \left(2a_{12} + a_{66}\right)s^2 - 2a_{26}s + a_{22} = 0 \tag{6}$$

where the a_{ij} are the elastic compliance coefficients, which can be written in terms of Young's moduli E_{ij}, Poisson's ratios v_{ij} and shear moduli G_{ij}. For an orthotropic material, a_{ij} are given as:

$$\begin{aligned} &a_{11} = \frac{1}{E_{11}} \quad a_{12} = -\frac{v_{21}}{E_{22}} = -\frac{v_{12}}{E_{11}} \quad a_{13} = -\frac{v_{31}}{E_{22}} = -\frac{v_{13}}{E_{11}} \quad a_{22} = \frac{1}{E_{22}} \quad a_{12} = -\frac{v_{32}}{E_{33}} = -\frac{v_{23}}{E_{22}} \\ &a_{33} = -\frac{1}{E_{33}} \quad a_{44} = \frac{1}{G_{23}} \quad a_{55} = \frac{1}{G_{13}} \quad a_{66} = \frac{1}{G_{12}} \quad a_{16} = a_{26} = a_{36} = 0 \end{aligned} \tag{7}$$

3 TWO-DIMENSIONAL ANISOTROPIC THERMOELASTICITY

In what follows, lower case *p* and *q* are used to denote points within the domain, Ω, and upper case *P* and *Q* are used to denote points on the boundary, *S*. The BIE for anisotropic thermoelasticity has the same form as equation for isotropic thermoelasticity. However, the equivalent body force term for isotropy is replaced by the equivalent body force term for anisotropy, X_i' namely,

$$c_{ij}(P)u_i(P)+\int_s u_i(Q)T_{ij}(P,Q)dS=\int_s t_i(Q)U_{ij}(P,Q)dS+\int_\Omega X_i'(q)U_{ij}(p,q)d\Omega \tag{8}$$

where *i,j* denote Cartesian components, and $T_{ij}(P,Q)$ and $U_{ij}(P,Q)$ represent the traction and displacement fundamental solutions at a boundary point *Q* due to a unit load placed at location *P*. The term $C_{ij}(P)$ is generally a function of the geometry variation at the boundary point *P*.

In Eq. (8) the displacement fundamental solution $U_{ij}(p,q)$ is now

$$U_{ij}(p,q)=2\,\mathrm{Re}\left[p_j A_{i1}\log z_1+q_j A_{i2}\log z_2\right]\qquad i,j=1,2 \tag{9}$$

and the corresponding traction fundamental solution is,

$$T_{i1}(p,q)=2n_1\,\mathrm{Re}\left[\frac{s_1^2A_{i1}}{z_1}+\frac{s_2^2A_{i2}}{z_2}\right]-2n_2\,\mathrm{Re}\left[\frac{s_1A_{i1}}{z_1}+\frac{s_2A_{i2}}{z_2}\right] \tag{10a}$$

$$T_{i2}(p,q)=-2n_1\,\mathrm{Re}\left[\frac{s_1A_{i1}}{z_1}+\frac{s_2A_{i2}}{z_2}\right]+2n_2\,\mathrm{Re}\left[\frac{A_{i1}}{z_1}+\frac{A_{i2}}{z_2}\right] \tag{10b}$$

n_i are the components of the unit outward normal at the field point *q*; and A_{ij} are complex constants obtained from the following matrix equation,

$$\left[\mathrm{Im}\{B_1\}\,\mathrm{Re}\{B_1\}\,\mathrm{Im}\{B_2\}\,\mathrm{Re}\{B_2\}\right]\begin{bmatrix}\mathrm{Re}\{A_{i1}\}\\ \mathrm{Im}\{A_{i1}\}\\ \mathrm{Re}\{A_{i2}\}\\ \mathrm{Im}\{A_{i2}\}\end{bmatrix}=\begin{bmatrix}\frac{-1}{4\pi} & \delta_{i2}\\ \frac{1}{4\pi} & \delta_{i2}\\ 0 & 0\\ 0 & 0\end{bmatrix} \tag{11}$$

where $\{B_1\}=\begin{bmatrix}1 & s_1 & p_1 & p_2\end{bmatrix}^T$; $\{B_2\}=\begin{bmatrix}2 & s_2 & q_1 & q_2\end{bmatrix}^T$ and δ_{jk} is the Kronecker delta.

Substituting X_i' in to Eq. (8) along with the additional thermal traction term, results in the integral equation for thermoelasticity, which, in the absence of body forces, can be written as,

$$c_{ij}(P)u_i(P)+\int_s u_i(Q)T_{ij}(P,Q)dS=\int_s t_i(Q)U_{ij}(P,Q)dS+\int_s \gamma_{ik}'n_k\theta U_{ij}(p,q)dS+\int_s \gamma_{ik}'\theta_{,k}U_{ij}(p,q)d\Omega \tag{12}$$

where, n_k is the unit outward normal at field point *Q*, θ is the temperature change, and,

$$\gamma_{ij}=C_{ijkl}\alpha_{kl} \tag{13}$$

And α_{kl} are the coefficients of linear expansion. C_{ijkl} are the material stiffness coefficients. In order to realize the full advantages of the boundary element method, it is important to transform the domain integral in Eq. (12) into surface integrals, thus rendering the equation a boundary only equation. This transformation has been achieved only quite recently through a direct domain mapping technique [22, 23]. In this method, the domain integral is mapped into a new coordinate system, $\bar{x}_i$, such that the new $\bar{x}_i$-coordinate system is related to the original Cartesian coordinate system by the following transformation,

$$\bar{x}_1 = \frac{\sqrt{\Delta}}{k_{11}} x_1 \tag{14}$$

$$\bar{x}_2 = x_2 - \frac{k_{12}}{k_{11}} x_1 \tag{15}$$

where $k_{ij}(i,j=1,2)$ are the heat conductivity coefficients, and $\Delta = k_{11}k_{22} - k_{12}^2 > 0$. Thus, the new transformed volume integral can now be expressed as,

$$(V.I)_j = \int_{\Omega} \gamma_{\bar{i}\bar{k}} \theta_{,\bar{k}} U_{\bar{i}\bar{j}} d\bar{\Omega} \tag{16}$$

The variables are now defined in the new mapped coordinate system, and $\gamma_{\bar{i}\bar{k}}$ is defined in matrix form as,

$$\gamma_{\bar{i}\bar{k}} = \begin{bmatrix} \gamma_{11} \dfrac{(-\gamma_{11}k_{12} + \gamma_{12}k_{11}}{\sqrt{\Delta}} \\ \gamma_{21} \dfrac{(-\gamma_{21}k_{12} + \gamma_{22}k_{11}}{\sqrt{\Delta}} \end{bmatrix} \tag{17}$$

The volume integral in Eq. (16) is analytically transformed into the following surface integral,

$$(V.I)_j = \int_s \left[(\gamma_{\bar{i}\bar{k}} Q_{\overline{ijk},t} \theta - \gamma_{\bar{i}\bar{k}} Q_{\overline{ijk}} \theta_{,t} + \gamma_{\bar{i}\bar{k}} R_{\overline{ijkt}} \theta_{,tt}) n_{\bar{t}} - \gamma_{\bar{i}\bar{k}} U_{\bar{i}\bar{j}} \theta n_{\bar{k}} \right] d\bar{S} \tag{18}$$

where

$$Q_{\overline{ijk}} = 2\,\mathrm{Re}\left\{ \frac{p_i A_{j\bar{1}} s_{\bar{k}\bar{1}} z_{\bar{1}} \log z_{\bar{1}}}{(s_{\bar{1}\bar{1}}^2 + s_{\bar{2}\bar{1}}^2)} + \frac{q_i A_{j\bar{2}} s_{\bar{k}\bar{2}} z_{\bar{2}} \log z_{\bar{2}}}{(s_{\bar{2}\bar{2}}^2 + s_{\bar{2}\bar{1}}^2)} \right\} \tag{19}$$

$$Q_{\overline{ijk},t} = 2\,\mathrm{Re}\left\{ \frac{p_i A_{j\bar{1}} s_{\bar{k}\bar{1}} s_{\bar{t}\bar{1}} z_{\bar{1}} \log z_{\bar{1}}}{(s_{\bar{1}\bar{1}}^2 + s_{\bar{2}\bar{1}}^2)} + \frac{q_i A_{j\bar{2}} s_{\bar{k}\bar{2}} s_{\bar{t}\bar{2}} z_{\bar{2}} \log z_{\bar{2}}}{(s_{\bar{2}\bar{2}}^2 + s_{\bar{2}\bar{1}}^2)} \right\} \tag{20}$$

$$R_{\overline{ijkt}} = 2\,\mathrm{Re}\left\{ \frac{p_i A_{j\bar{1}} s_{\bar{k}\bar{1}} (z_{\bar{1}}^2 \log z_{\bar{1}} - z_{\bar{1}}^2/2)}{4 s_{\bar{t}\bar{1}} (s_{\bar{1}\bar{1}}^2 + s_{\bar{2}\bar{1}}^2)} + \frac{q_i A_{j\bar{2}} s_{\bar{k}\bar{2}} (z_{\bar{2}}^2 \log z_{\bar{2}} - z_{\bar{2}}^2/2)}{4 s_{\bar{t}\bar{2}} (s_{\bar{2}\bar{2}}^2 + s_{\bar{2}\bar{1}}^2)} \right\} \tag{21}$$

and

$$S_{\bar{j}\bar{i}} = \begin{bmatrix} \dfrac{(k_{11} + s_1 k_{12})}{\sqrt{\Delta}} & \dfrac{(k_{11} + s_2 k_{12})}{\sqrt{\Delta}} \\ s_1 & s_2 \end{bmatrix} \tag{22}$$

Thus, the resulting BIE for two-dimensional anisotropic thermoelasticity by the exact transformation method (ETM) can be expressed as,

$$c_{ij}(P)u_i(P)+\int_s u_i(Q)T_{ij}(P,Q)dS=\int_s t_i(Q)U_{ij}(P,Q)dS+\int_s \gamma_{ik}n_k\theta U_{ij}(p,q)dS \\ +\int_{\bar{s}}\left[(\gamma_{\bar{i}\bar{k}}Q_{\bar{i}\bar{j}\bar{k},t}\theta-\gamma_{\bar{i}\bar{k}}Q_{\bar{i}\bar{j}\bar{k}}\theta_{,t}+\gamma_{\bar{i}\bar{k}}R_{\bar{i}\bar{j}kt}\theta_{,tt})n_t-\gamma_{\bar{i}\bar{k}}U_{\bar{i}\bar{j}}\theta n_{\bar{k}}\right]d\bar{S} \tag{23}$$

The integrals in Eq. (23) pose no numerical problems because they are weakly singular at most. However, care must still be taken to avoid discontinuities which arise due to the geometry of the domain. It has been shown [29, 19] that such discontinuities can be avoided provided that,

a) For a simply connected convex domain, the range of functions involving z are limited such that,

$$0\prec\arg(z)\le 2\pi \tag{24}$$

b) For a simply connected but non-convex domain, the range of functions involving z are limited such that,

$$\Phi-2\pi\prec\arg(z)\le\Phi \tag{25}$$

where, $\Phi\ [0,2\pi]$ is the angle between the outward normal and the x_1-axis.

c) For multiply connected domains, the domain is cut into infinitesimal strips, resulting in an extra line integral in Eq. (23) such that it now becomes,

$$c_{ij}(P)u_i(P)+\int_s u_i(Q)T_{ij}(P,Q)dS=\int_s t_i(Q)U_{ij}(P,Q)dS+\int_s \gamma_{ik}n_k\theta U_{ij}(p,q)dS \\ +\int_{\bar{s}}\left[(\gamma_{\bar{i}\bar{k}}Q_{\bar{i}\bar{j}\bar{k},t}\theta-\gamma_{\bar{i}\bar{k}}Q_{\bar{i}\bar{j}\bar{k}}\theta_{,t}+\gamma_{\bar{i}\bar{k}}R_{\bar{i}\bar{j}kt}\theta_{,tt})n_t-\gamma_{\bar{i}\bar{k}}U_{\bar{i}\bar{j}}\theta n_{\bar{k}}\right]d\bar{S}+\sum_{n=1}^{m}\int_{l_{2n-1}}^{l_{2n-2}}L_j(\zeta_1)d\zeta_1 \tag{26}$$

where, m is the number of times that the domain is intersected by the negative ζ_1-axis, and $L_j(\zeta_1)$ is defined as,

$$L_j(\zeta_1)=4\pi\theta\gamma_{\bar{i}\bar{k}}\left(\frac{k_{12}}{k_{11}}\mathrm{Im}\left\{\frac{p_iA_{j1}s_{\bar{1}\bar{1}}s_{\bar{k}\bar{1}}}{(s_{\bar{1}\bar{1}}^2+s_{\bar{2}\bar{1}}^2)}+\frac{q_iA_{j2}s_{\bar{1}\bar{2}}s_{\bar{k}\bar{2}}}{(s_{\bar{2}\bar{2}}^2+s_{\bar{1}\bar{2}}^2)}\right\}+\frac{\sqrt{\Delta}}{k_{11}}\mathrm{Im}\left\{\frac{p_iA_{j1}s_{\bar{2}\bar{1}}s_{\bar{k}\bar{1}}}{(s_{\bar{1}\bar{1}}^2+s_{\bar{2}\bar{1}}^2)}+\frac{q_iA_{j2}s_{\bar{2}\bar{2}}s_{\bar{k}\bar{2}}}{(s_{\bar{2}\bar{2}}^2+s_{\bar{1}\bar{2}}^2)}\right\}\right) \\ -4\pi\gamma_{\bar{i}\bar{k}}\left(\frac{k_{12}}{k_{11}}\theta_{,1}+\frac{\sqrt{\Delta}}{k_{11}}\theta_{,2}\right)\mathrm{Im}\left\{\frac{p_iA_{j1}s_{\bar{k}\bar{1}}}{(s_{\bar{1}\bar{1}}^2+s_{\bar{2}\bar{1}}^2)}+\frac{q_iA_{j2}s_{\bar{k}\bar{2}}}{(s_{\bar{2}\bar{2}}^2+s_{\bar{1}\bar{2}}^2)}\right\}+\theta_{,ii}\pi\zeta_1^2\gamma_{\bar{i}\bar{k}}\left(\begin{array}{l}\frac{k_{12}}{k_{11}}\mathrm{Im}\left\{\frac{p_iA_{j1}s_{\bar{k}\bar{1}}}{s_{\bar{1}\bar{1}}(s_{\bar{1}\bar{1}}^2+s_{\bar{2}\bar{1}}^2)}+\frac{q_iA_{j2}s_{\bar{k}\bar{2}}}{s_{\bar{1}\bar{2}}(s_{\bar{2}\bar{2}}^2+s_{\bar{1}\bar{2}}^2)}\right\}\\+\frac{\sqrt{\Delta}}{k_{11}}\mathrm{Im}\left\{\frac{p_iA_{j1}s_{\bar{k}\bar{1}}}{s_{\bar{2}\bar{1}}(s_{\bar{1}\bar{1}}^2+s_{\bar{2}\bar{1}}^2)}+\frac{q_iA_{j2}s_{\bar{k}\bar{2}}}{s_{\bar{2}\bar{2}}(s_{\bar{2}\bar{2}}^2+s_{\bar{1}\bar{2}}^2)}\right\}\end{array}\right) \\ -4\pi\theta\left(\frac{k_{12}}{k_{11}}\gamma_{\bar{i}\bar{1}}+\frac{\sqrt{\Delta}}{k_{11}}\gamma_{\bar{i}\bar{2}}\right)\mathrm{Im}\left\{p_iA_{j1}+q_iA_{j2}\right\} \tag{27}$$

Eq. (27) is analytically exact for any physical domain. However, for thermoelasticity problems, temperature data is required along the negative ζ_1-axis for every source point along the boundary. This is highly undesirable since it greatly increases the amount of computation required for the problem solution. Fortunately, this line integral can be avoided altogether through the selective use of sub-regioning to transform the multiply connected domain into a finite, and generally small, number of simply connected non-convex domains, so that the much more simple argument of Eq. (25) can be employed (see Fig. 1). The form of the discretized BIE, and the numerical procedures for solving it are the same for anisotropy as they are for isotropy, hence they will not be elaborated on further.

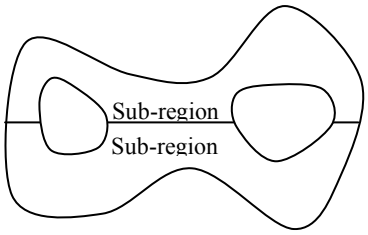

Fig.1
A multiply-connected domain divided into two simply connected non-convex sub-regions.

4 TWO –DIMENSIONAL LINEAR ELASTIC FRACTURE MECHANICS ANALYSIS

The BIE method for two-dimensional homogeneous anisotropic thermoelasticity discussed in the previous section can be applied to the analysis of crack problems without requiring any approximation or further modification. All that is required are special 'crack-tip' elements to model the crack, and appropriate formulae to calculate the stress intensity factors from the computed displacements and tractions.

In order to model anisotropic problems with a general crack, sub-regioning of the solution domain may be employed. The sub-regions are chosen such that the crack, of arbitrary orientation, lies along the sub-region interface. The nodes at this interface boundary are bonded along the un-cracked portion, and are free along the crack face (see Fig. 2).

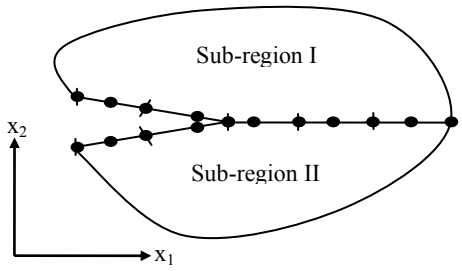

Fig.2
An arbitrary cracked body after sub-regioning.

with the crack being modeled using quarter-point elements at the crack-tip, the stress intensity factors can be obtained directly from the computed displacements and tractions at the nodes of these elements, using either the 'traction formula',

$$K_I = t_2^{-A}\sqrt{2\pi l} \tag{28a}$$

$$K_{II} = t_1^{-A}\sqrt{2\pi l} \tag{28b}$$

or the 'displacement formula',

$$\begin{bmatrix} K_I \\ K_{II} \end{bmatrix} = \frac{\sqrt{(\pi/2l)}}{Det[D]} \begin{bmatrix} D_{22} & -D_{12} \\ -D_{21} & D_{22} \end{bmatrix} \begin{Bmatrix} (-u_1^C + 4u_1^B - 3u_1^A) \\ (-u_2^C + 4u_2^B - 3u_2^A) \end{Bmatrix} \tag{29}$$

as derived by [13]. In Eqs. (28) and (29) the superscripts indicate the nodes of the crack-tip elements as shown in Fig. 3. The computed traction at the crack-tip, t_j^{-A} is related to the physical traction, t_j^A as follows,

$$t_j^{-A} = \lim_{r\to 0} t_j^A \sqrt{\frac{r}{l}} \tag{30}$$

and

$$Det[D] = (D_{11}D_{22} - D_{21}D_{12}) \tag{31}$$

where

$$\begin{aligned} D_{11} &= \mathrm{Im}\left[\frac{s_2 p_1 - s_1 p_2}{s_1 - s_2}\right] \qquad D_{12} = \mathrm{Im}\left[\frac{p_1 - p_2}{s_1 - s_2}\right] \\ D_{21} &= \mathrm{Im}\left[\frac{s_2 q_1 - s_1 q_2}{s_1 - s_2}\right] \qquad D_{12} = \mathrm{Im}\left[\frac{q_1 - q_2}{s_1 - s_2}\right] \end{aligned} \tag{32}$$

The displacement formula requires significantly more computation than the traction formula, and is known to be more sensitive to the size of the crack-tip element, *l* [13]. However, the use of both formulae provides a useful cross-check of the results, and good agreement can also be an indicator of good mesh design.

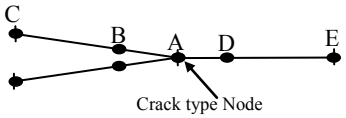

Fig.3
Node symbols for crack-tip elements.

5 THERMOELASTIC FRACTURE MECHANICS ANALYSIS IN PLANE ANISOTROPY

The goal of the present study is to determine the effect of varying material properties on the value of the stress intensity factors, K_I and K_{II}, for anisotropic plates containing cracks and subjected to a temperature change. This section outlines the scope of the parametric study carried out to examine these effects.

For the two-dimensional anisotropic thermoelastic fracture mechanics study performed here, the basic physical problem is that of a rectangular plate with a crack, whereupon the crack opens as a result of a uniform temperature drop. The plate is constrained in the vertical direction along the top and bottom edges, and constrained in the horizontal direction at the middle of the bottom edge (see Fig. 4). These boundary conditions allow the plate to expand or contract in the horizontal direction but not in the vertical direction, while also eliminating rigid body motion in the numerical analysis. In all cases, the plates are cooled by a temperature of $100^{\circ}C$, and the height to width ratio, *H/W*, is 2 (see Fig. 4).

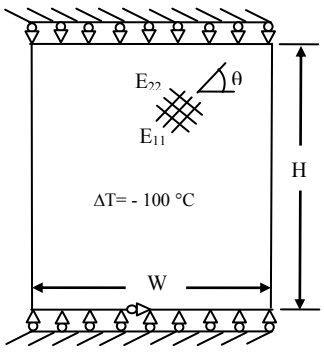

Fig.4
Boundary conditions for problem analysis.

The three basic types of cracked plates investigated in this study are (a) an edge cracked plate (see Fig. 5), (b) a plate with a double edge-crack (see Fig. 6) and (c) a plate with symmetric cracks emanating from a circular hole (see Fig.7). Also, for the BEM analysis, relative crack lengths considered are $a/W = 0.1, 0.2, 0.3, 0.4, 0.5$, where 'a' is the crack length.

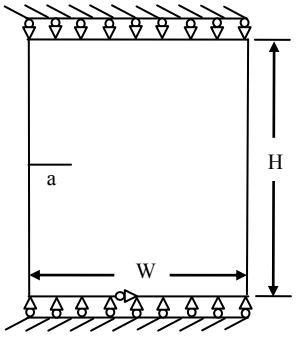

Fig.5
Plate with an edge-crack.

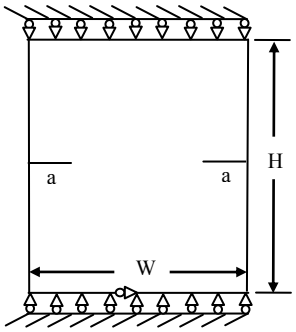

Fig.6
Plate with double edge-crack.

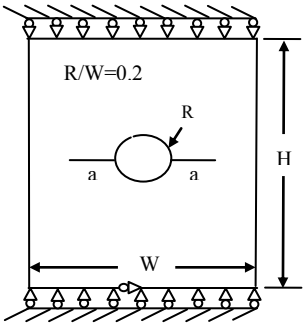

Fig.7
Plate with symmetric cracks emanating from a central hole.

5.1 Material properties

For two-dimensional anisotropy in plane stress, four elastic constants are normally required to fully define the material, namely E_{11}, E_{22}, G_{12} and v_{12} . In order to reduce the number of runs required in the parametric study, an alternative method of representing the material properties was used [2], whereby these four elastic constants can be related to a pair of new material parameters, η_1 and η_2 , as follows,

$$\eta_1\eta_2 = \sqrt{\frac{E_{11}}{E_{22}}} \qquad \eta_1 + \eta_2 = \sqrt{2\left(\sqrt{\frac{E_{11}}{E_{22}}} + \frac{E_{12}}{2G_{12}} - \nu_{12}\right)} \tag{33}$$

In anisotropy, the angle between the global Cartesian coordinate system, and the material principal Cartesian coordinate system, is very important in defining the properties of a material. The range of this material property angle, θ, was chosen to be between 0 and 90 degrees, and the following five values are considered, $\theta = 0, 30, 45, 60, 90$.

So far, thermal properties have not been represented for the parametric study. This requires the creation of a third material parameter representing the ratio of the material coefficients of linear expansion, α_{11} and α_{22}, in the principal directions. This parameter, which will be called η_3 for convenience, is defined as,

$$\eta_3 = \frac{\alpha_{22}}{\alpha_{11}} \tag{34}$$

Therefore, α_{11} is set to be $0.01\times10^{-6} m/m/^{\circ}C$ throughout this study. In order to determine the effect of varying η_3, the stress intensity factors were computed for numerous values of η_3, for $\theta = 0, 45, 90$ and for the material parameter extremes, $[\eta_1, \eta_2] = [2, 0.5]$ and $[\eta_1, \eta_2] = [7, 1]$. The stress intensity factors, K_I and K_{II}, are all normalized to produce the normalized stress intensity factors, K_I^* and K_{II}^*, defined as follows:

$$K_I^* = \frac{K_I}{E_{11}\eta_3\alpha_{11}\Delta T\sqrt{\pi a}} \qquad K_{II}^* = \frac{K_{II}}{E_{11}\eta_3\alpha_{11}\Delta T\sqrt{\pi a}} \tag{35}$$

6 NUMERICAL RESULTS AND DISCUSSION

This section presents the stress intensity factor (SIF) results obtained from the parametric study outlined in the previous section. The general trends resulting from variation of the material parameters η_1 and η_2, which are used to define the anisotropic properties of the material, are first presented. These parameters are directly related to the material elastic constants, and thus will give an indication of the overall effect that variation of the mechanical properties has on the SIFs for anisotropic plates under thermal loads. The results of varying the orientation of the material properties are presented next, and the effect on the value of the SIFs is discussed. This is followed by a look at the effect of crack length on the SIFs for each plate geometry.

It is important to note that, in general, only the results for the mode-I normalized stress intensity factor, K_I^*, are plotted and discussed. Values for the mode-II normalized stress intensity factor, K_{II}^*, were typically an order of magnitude smaller than K_I^* and are therefore only of secondary importance.

6.1 Effects of material properties, η_1 and η_2

These results are shown for the edge-crack case in Figs. 8 and 9. It can be seen from these graphs that, in all cases, for values of η_3 greater than +5, or less than -5, the normalized stress intensity factors change very little. Therefore, any results obtained should be directly applicable to all materials with η_3 greater than +10, or less than -10. Therefore, for the purpose of efficiency, only the case of $\eta_3 = 30$ is considered for further analysis.

The variations of the normalized stress intensity factor, K_I^*, with varying values of η_1 and η_2 for a uniformly cooled plate can be seen in Figs. 10-11. From these figures one can clearly see that regardless of material property angle, θ, or relative crack length, a/W, the normalized SIF, K_I^* and K_{II}^* decreases as either of the material parameters, η_1 or η_2, is increased. Note that independently increasing either material parameter η_1 or material parameter η_2 corresponds to an increase in the "degree of anisotropy" of the material properties. Therefore, it is fair to say that, in general, the normalized stress intensity factor, K_I^* and K_{II}^* decreases as the material becomes "more anisotropic" and this is true of all three crack cases in this study.

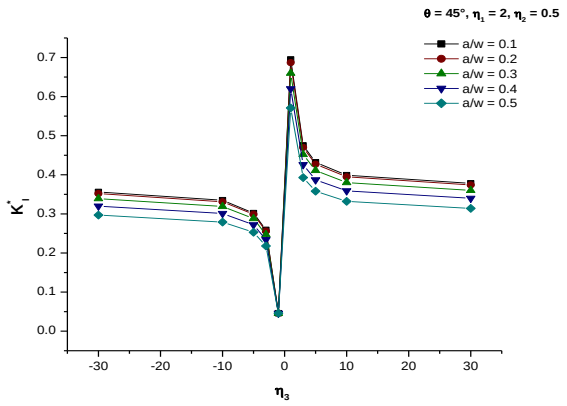

Fig.8
Variation of the normalized stress intensity factors, K_I^* with (a) normalized crack length, a/W , and (b) material parameter η_3, for a uniformly cooled plate with an edge-crack; $\theta = 45^\circ, \eta_1 = 2$, $\eta_2 = 0.5$.

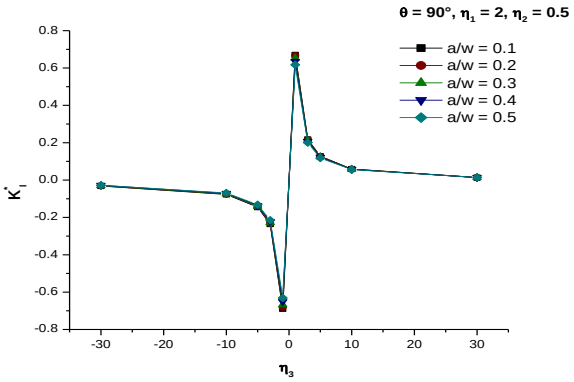

Fig.9
Variation of the normalized stress intensity factors, K_I^* with (a) normalized crack length, a/W , and (b) material parameter η_3, for a uniformly cooled plate with an edge-crack; $\theta = 90^\circ, \eta_1 = 2$, $\eta_2 = 0.5$.

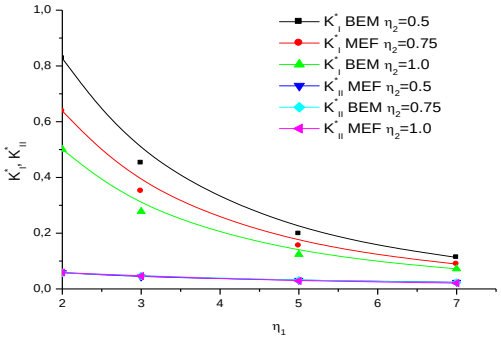

Fig.10
Variation of the normalized stress intensity factors, K_I^* and K_{II}^* with material parameter η_1, for plate with symmetric cracks emanating from a central hole.

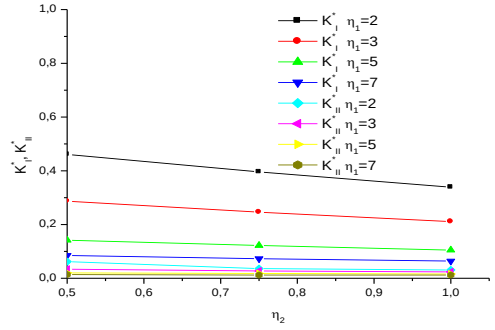

Fig.11
Variation of the normalized stress intensity factors, K_I^* and K_{II}^* with material parameter η_2, for plate with symmetric cracks emanating from a central hole.

6.2 Effects of material property angle, θ

The variation of normalized SIF, K_I^*, with varying material property angle, θ, for various material properties and crack lengths is shown in Figs. 12 and 13. Before discussing the results, it is important to recall the physical boundary conditions which are applied to the plates (see Fig. 4). As described in the previous section the plates are constrained at the top and bottom edges, and it is this constraint which induces the crack to open as the plate is cooled. When $\theta = 0$, E_{11} is oriented in the horizontal direction, and α_{22} is oriented in the vertical direction. This means that when $\theta = 0$ the plates are most stiff in the horizontal direction, and maximum shrinkage of the plates is occurring in the vertical direction which is the least stiff. As θ increases, both E_{11} and α_{22} are rotated counterclockwise until $\theta = 90$, where now E_{11} is vertical, and α_{22} is horizontal. Therefore, $\theta = 90$ corresponds to a condition of maximum stiffness in the vertical direction and maximum shrinkage in the horizontal direction. For all three crack cases, the general trend observed is that the normalized SIF, K_I^*, is maximum at $\theta = 0$ and decreases in a sinusoidal fashion to a minimum value at $\theta = 90$. The maximum value at $\theta = 0$ is expected in this situation since it corresponds both to maximum vertical shrinkage and minimum vertical stiffness. Thus the crack opens by the maximum amount, yielding the maximum value of K_I^*. At $\theta = 90$, the opposite situation arises. When $\theta = 90$, shrinkage occurs mainly in the horizontal direction where the plate is free to expand and for contract. There is the minimum amount of shrinkage in the vertical direction, and the maximum amount of stiffness in that direction, resulting in relatively low stresses at the crack-tip, and the minimum value of K_I^*. It is expected that if the material properties were rotated further, from $\theta = 90$ to $\theta = 180$, the observed trends would be mirrored, and the normalized SIF, K_I^*, would increase back to a maximum at $\theta = 180$, and this cyclic behavior should continue through to $\theta = 360$.

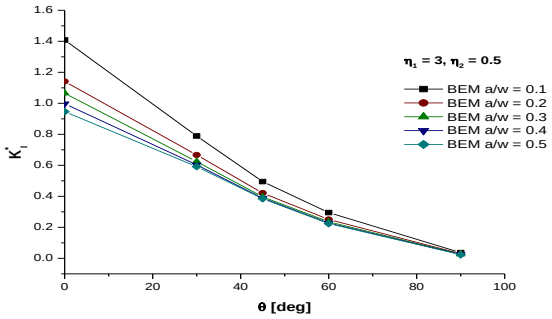

Fig.12
Normalized stress intensity factors, K_I^*, with varying material angle, θ, and normalized crack length, a/W, for a uniformly cooled plate with an edge-cracks; $\eta_1 = 3, \eta_2 = 0.5$.

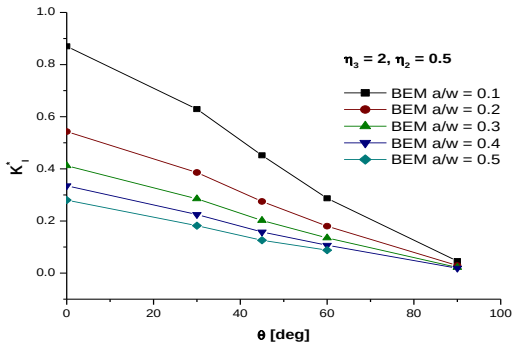

Fig.13
Normalized stress intensity factors, K_I^*, with varying material angle, θ, and normalized crack length, a/W, for a uniformly cooled plate with symmetric edge-cracks emanating from a central hole; $\eta_1 = 2$.

6.3 Effects of crack length, a/W

Although the three crack cases analyzed in this study all exhibit the same behavior for varying material parameters, η_1, and η_2, and varying material property angle, θ, there are some differences in observed trends as it relates to crack length. Certain cases exhibit a greater dependence of the normalized stress intensity factors on crack length.

The variations of K_I^* and K_{II}^* with relative crack length, a/W, for the three crack cases are shown in Figs. 14, 15 and 16. It can be seen in these figures that there is a trend of decreasing K_I^* and K_{II}^* with increasing relative crack length, and this trend is generally present for any combination of material properties, η_1, and η_2, or material property angle, θ. It is also evident from the results that, for a given set of material properties, the decrease of K_I^* with crack length is relatively more dramatic for the geometric cases with a hole or a semi-circular notch. This is particularly so at the smaller relative crack lengths where the effects of the stress concentrations of these geometric discontinuities are still apparent, and is therefore to be expected.

It is worth noting that although the normalized stress intensity factor, K_I^* may decrease with increasing relative crack length, a/W, the absolute value of K_I actually increases with crack size in all cases.

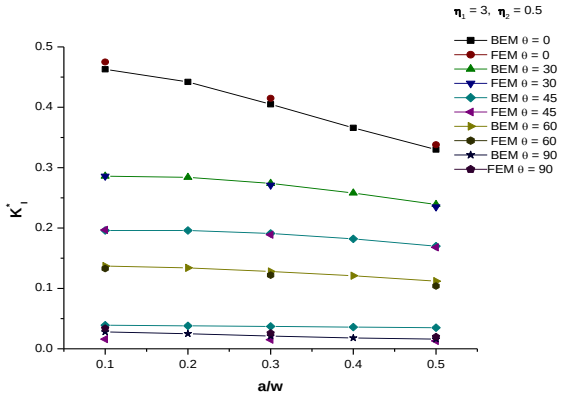

Fig.14
Normalized stress intensity factors, K_I^*, with varying material angle, θ, and normalized crack length, a/W, for a uniformly cooled plate with an edge-cracks; $\eta_1 = 3, \eta_2 = 0.5$.

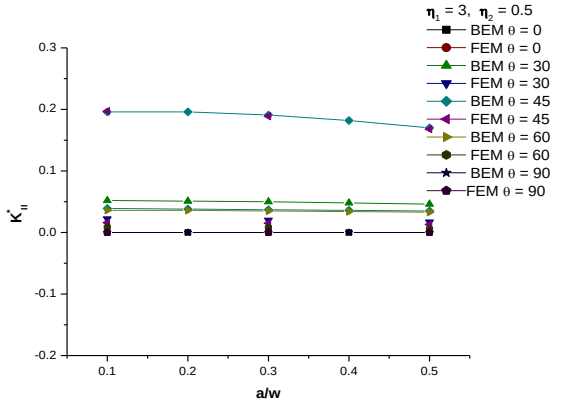

Fig.15
Normalized stress intensity factors, K_{II}^*, with varying material angle, θ, and normalized crack length, a/W, for a uniformly cooled plate with an edge-cracks; $\eta_1 = 3, \eta_2 = 0.5$.

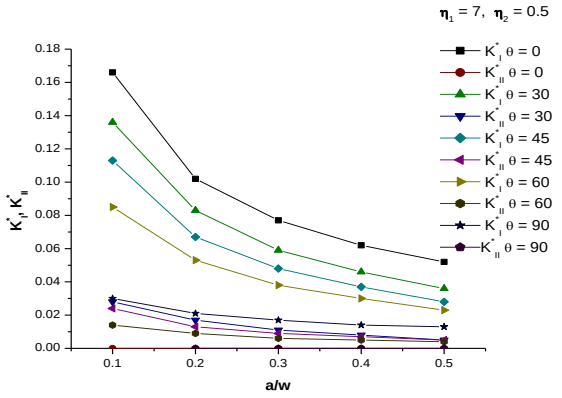

Fig.16
Normalized stress intensity factors, K_I^* and K_{II}^* with varying material angle, θ, and normalized crack length, a/W, for a uniformly cooled plate with double edge-cracks; $\eta_1 = 7, \eta_2 = 0.5$.

7 CONCLUSIONS

A two-dimensional thermoelastic fracture mechanics analysis of anisotropic bodies has been performed using the boundary element method (BEM). There are a few general conclusions which can be made from the results obtained.

First, as the material becomes 'more anisotropic', or in other words as η_1, and η_2 deviate further from unity, the value of the normalized stress intensity factor (SIF), K_I^*, decreases for a given crack size. Second, for the boundary conditions used in this study, as the material property angle, θ, is increased, K_I^* also decreases in a sinusoidal manner from $\theta = 0$ to $\theta = 90$ degrees. It is expected that K_I^* will continue to vary in a sinusoidal fashion from $\theta = 90$ degrees to $\theta = 360$ degrees. Third, the normalized stress intensity factor, K_I^*, in general, decreases with increasing relative crack length, for a given set of anisotropic material properties for the geometric cases considered. There is an exception however for the plate with the central-crack, where K_I^* was found, for all practical purposes, not to change with relative crack length. As expected, the presence of geometric discontinuities such as a hole or a notch was found to have a more pronounced influence on the magnitude, and the rate of change, of K_I^*, particularly at smaller relative crack lengths.

This study has shown that BEM is a quick and efficient numerical tool for the analysis of two-dimensional cracked anisotropic bodies under thermal loads. It has been found to be a much more efficient alternative to FEM for such problems.

REFERENCES

[1] Sih G.C., Paris P.C., Irwin G.R., 1965, On cracks in rectilinearly anisotropic bodies, *International Journal of Fracture Mechanics* **1**: 189-203.

[2] Bowie O.L., Freese C.E., 1972, Central crack in plane orthotropic rectangular sheet, *Journal of Fracture Mechanics* **1**: 49-58.

[3] Ghandi K.R., 1972, Analysis of an inclined crack centrally placed in an orthotropic rectangular plate, *Journal of Strain Analysis* **7**: 157-162.

[4] Rizzo F.J., Shippy D.J., 1970, A method for stress determination in plane anisotropic elastic bodies, *Journal of Composite Materials* **4**: 36-61.

[5] Snyder M.D., Cruse T.A., 1975, Boundary-integral equation analysis of cracked anisotropic plates, *International Journal of Fracture* **11**: 315-328.

[6] Sollero P., Alliabadi M.H., 1995, Anisotropic analysis of cracks in composite laminates using the dual boundary element method, *Composite Structures* **31**: 229-237.

[7] Pan E., 1997, A general boundary element analysis of 2-D linear elastic fracture mechanics, *International Journal of Fracture* **88**: 41-59.

[8] Haj-Ali R., Wei B. S., Johnson S., El-Hajjar R., 2008, Thermoelastic and infrared-thermography methods for surface strains in cracked orthotropic composite materials, *Engineering Fracture Mechanics* **75**(1): 58-75.

[9] Shiah Y. C., Tan C. L., 2000, Fracture mechanics analysis in 2-D anisotropic thermoelasticity using BEM, *Computer Modeling in Engineering & Sciences* **1**(3): 91-99.

[10] Pasternak I., 2012, Boundary integral equations and the boundary element method for fracture mechanics analysis in 2D anisotropic thermoelasticity, *Engineering Analysis with Boundary Elements* **36**(12): 1931-1941.

[11] Ju S. H., Rowlands R. E., 2003, Thermoelastic determination of K_I and K_{II} in an orthotropic graphite–epoxy composite, *Journal of Composite Materials* **37**(22): 2011-2025.

[12] Dag S., 2006, Thermal fracture analysis of orthotropic functionally graded materials using an equivalent domain integral approach, *Engineering Fracture Mechanics* **73**(18): 2802-2828.

[13] Tan C.L., Gao Y.L., 1992, Boundary element analysis of plane anisotropic bodies with stress concentrations and cracks, *Composite Structures* **20**: 17-28.

[14] Portela A., Aliabadi M.H., Rooke D.P., 1991, Efficient boundary element analysis of sharp notched plates, *International Journal for Numerical Methods in Engineering* **32**: 445-470.

[15] Sollero P., Alliabadi M.H., 1993, Fracture mechanics analysis of anisotropic plates by the boundary element method, *International Journal of Fracture* **64***:* 269-284.

[16] Aliabadi M.H., Cartwright D.J., Rooke D.P., 1989, Fracture-mechanics weight functions by the removal of singular fields using boundary element analysis, *International Journal of Fracture* **40**: 271-284.

[17] Portela A., Aliabadi M.H., Rooke D.P., 1991, Efficient boundary element analysis of sharp notched plates, *International Journal for Numerical Methods in Engineering* **32**: 445-470.
[18] Solkonikoff I.S., 1956, *Mathematical Theory of Elasticity,* McGraw-Hill, New York.
[19] Zhang J.J., Tan C.L., Afagh F.F., 1996, A general exact transformation of body- force volume integral in BEM for 2D anisotropic elasticity, *Computational Mechanics* **19**: 1-10.
[20] Zhang J.J., Tan C.L., Afagh F.F., 1997, Treatment of body-force volume integrals in BEM by exact transformation for 2-D anisotropic elasticity, *International Journal for Numerical Methods in Engineering* **40**: 89-109.
[21] Pape D.A., Banerjee P.K., 1987, Treatment of body forces in 2D electrostatic BEM using particular integrals, *Transactions of the ASME* **54**: 866-871.
[22] Shiah Y.C., Tan C.L., 1997, BEM treatment of two-dimensional anisotropic field problems by direct domain mapping, *Engineering Analysis with Boundary Elements* **20**: 347-351.
[23] Shiah Y.C., Tan C.L., 1999, Exact boundary integral transformation of the thermoelastic domain integral in BEM for general 2D anisotropic elasticity, *Computational Mechanics* **23**: 87-96.
[24] Shiah Y.C., Tan C.L., 2000, Determination of interior point stresses in two dimensional BEM thermoelastic analysis of anisotropic bodies, *International Journal of Solids and Structures* **37**: 809-829.
[25] Shiah Y .C., Tan C.L., 2000, Fracture mechanics analysis in 2-D anisotropic thermoelasticity using BEM, *Computer Modeling in Engineering & Sciences* **3**: 91-99.
[26] Deb A., Banerjee P.K., Wilson R.B., 1991, Alternate BEM formulations for 2- and 3-D anisotropic thermoelasticity, *International Journal of Solids and Structures* **27**: 1721-1738.
[27] Deb A., Banerjee P.K., 1991, Multi-domain two- and three-dimensional thermoelasticity by BEM, *International Journal for Numerical Methods in Engineering* **32**: 991-1008.
[28] De Saxce G., Kang C.H., 1992, Application of the hybrid mongrel displacement finite method to the computation of stress intensity factors in anisotropic material, *Engineering Fracture Mechanics* **41**: 71-83.
[29] Zhang J.J., Tan C.L., Afagh F.F., 1996, An argument redefinition procedure in the BEM for 2D anisotropic electrostatics with body forces, *Processing Symposium on Mechanics in Design*, Toronto, Meguid.